8-7-2019

Modeling Composite Cytoskeletal Networks using Effective Medium Theory

Jacob Wales
jfw7052@rit.edu

Modeling Composite Cytoskeletal Networks using Effective Medium Theory

Thesis submitted to the Mathematics department of the Gosnell College of Science at the Rochester Institute of technology for fulfillment of the **Masters of Science in Applied and Computational Mathematics** degree.

Jacob Wales

Date: August 7, 2019

Abstract

The mechanical response of most living cells arises from their cytoskeleton, a polymeric scaffold made of different types of biopolymers and associated crosslinking proteins. We used rigidity percolation theory to devise a set of models using an effective medium approach to study the mechanical properties of cytoskeleton-like networks. We first successfully recreated a model which obtains the mechanical response of a disordered network of a single filament type, given the constitutive material properties of individual filaments and the network geometry. In this model, wherever two filaments cross they are crosslinked together, and these crosslinkers allow for energy free rotation of filaments but not translation, so the filaments cannot slide along one another. We then extended our approach for a model which involved "phantom" cosslinkers. At crosslinking nodes involving these crosslinkers, only a maximum of two filaments can be crosslinked together at a binding site, and if a third filament were to go through the connection, it would simply pass through and not be physically bound by the crosslinker. Although phantom cross-linkers have been used in computer simulations in the past, they have not been previously investigated analytically, including in a mean field theory. With both of these models involving only one filament and

crosslinker type, we were then able to devise our main goal of extending the effective medium approach to composite networks of two types of filaments and crosslinkers. Specifically, this model involves two networks, for example an actin network and a microtubule network, and places weak spring-like interactions between filaments belonging to the two to resemble various types of interactions; for example weaker interactions represent entanglement and stronger springs to represent actual crosslinking between the two networks. With this new model we are able to define composite networks made of individual networks of stiff and soft filaments, and any combination of the two types of crosslinkers mentioned previously, with varying levels of interaction between the networks. Our results may provide new insights into the collective mechanical response of composite networks found in the cytoskeleton and design principles for engineered networks that mimic the cytoskeleton.

Committee Approval

Approved: _____

Dr. Mathew Hoffman, Ph.D. Date

Director of the Masters Program in Computational and Applied Math

Approved: _____

Dr. Moumita Das, Ph.D. Date

Thesis Advisor, Committee Member

Approved: _____

Dr. George Thurston, Ph.D. Date

Committee Member

Approved: _____

Dr. David Ross, Ph.D. Date

Committee Member

Contents

0.1 Introduction

Biological cells are robust systems able to withstand incredible external stresses, due in large part to the cytoskeleton. The cytoskeleton is a network of biopolymers and consists of a wide variety of filament types that are crosslinked via different types of crosslinking proteins. The mechanical responses of these structures are predominantly determined by three of such fibers, stiff microtubules, more flexible actin (specifically F-actin), and intermediate filaments between them [7]. The study of these networks can be difficult when examining an entire cell, due to the inherent complexity of the cell as a whole. Often, reconstituted in-vitro versions of cytoskeletal networks are created instead to better understand their mechanical properties. The most heavily studied of these reconstituted networks consists of a crosslinked network of actin filaments. The actin filaments, along with microtubules, are known to be semiflexible, i.e. both the actions of stretching and bending these filaments requires a non-negligible amount of energy. These networks have exhibited interesting responses in both linear and non-linear deformation regimes [7, 4, 5]. Other studies have included the addition of microtubules to these reconstituted networks, and this proves to promote stiffening as well as enable the cytoskeleton to withstand significantly more

compression [7]. There are numerous unexplored aspects of such composite networks, and one of the significant discoveries is the idea that the behavior of cytoskeletal networks depends on the construction and composition of the network itself, as well as the properties of the individual filaments which make it up [7].

We have chosen to explore this idea further. Our initial goal was to be able to make predictions about the rheological properties of a cytoskeleton-like network being only given the construction and filaments which it is composed of. Attempts at this idea have successfully been done using simulations [1] [3], however they apply to specific constructions, having to be re-evaluated for any change in network construction or filament parameter. It is because of this that we wanted to be able to make these predictions completely analytically, and formulate a generalized model which can be easily applied to a variety of possible constructions and filaments combinations.

With this goal in mind we decided to employ an effective medium approach through the lens of rigidity percolation theory. This approach has been proven an effective tool for various single network constructions, from a simple network of Hookean springs [6], to a network of semiflexible polymers [4, 5], however the approach has not been applied to a composite network

structure. We have successfully been able to extend this theory to both a new variety of single network, as well a composite network structure made up of two interacting networks of different filament types.

0.2 Model/Methods

0.2.1 Theory

With our goal in mind, we decided to structure our model as a composite network system composed of two interacting disordered networks, each of a different filament type. We primarily studied these networks through a framework known as Rigidity Percolation Theory [6, 4, 5]. The main idea behind this theory is to be able to comment on the rigidity of a network structure based on the number of bonds present. To illustrate this idea, consider a complete, ordered triangular lattice made up of springs as seen in the paper by Feng et. al. [6]. Assume now that we begin slowly removing some of the bonds from the network. Naturally, as we keep removing bonds we will eventually reach a point where the network is no longer rigid, meaning there must be some critical threshold of bond occupation probability required for our network to maintain rigidity. This critical threshold is known as the

rigidity percolation threshold, or p_{cen}, which for a network of springs happens to be $2d/z$, where d is the dimension and z is the number of nearest neighbor connections. For our triangular lattice, this happens to be at $\frac{2}{3}$ [6]. This means that, given a triangular network of springs, if we observe $\leq \frac{2}{3}$ of the bonds present, the network is nonrigid.

We have chosen to use rigidity percolation theory as our methodology to study these networks as it provides the basis for the implementation of an effective medium approach to model the networks. A full description of this process is contained in a subsequent section of this paper, however the core idea is to determine an ordered network, known as the effective medium, which demonstrates the same average responses when subjected to mechanical stresses as the original disordered system [6][4][5]. We use this approach to study mechanical response of various disordered, individual and composite, network constructions.

0.2.2 Single Networks

Spring Network

Previous work has been done to show the effectiveness of using an effective medium approach on disordered networks of a single filament type [6][4][5].

We began by reconstructing two of these models, the first of which being a disordered network of spring-like filaments as depicted in [6]. To create the network, we begin with a complete (containing all filaments) triangular lattice. Wherever two filaments intersect, which happens to be at each lattice point, we place a crosslink that allows for free rotation but prevents translation. This serves to allow the filaments to rotate without sliding along each other. To then add sufficient disorder to the network, we randomly remove bonds with a probability of $1-p$. This is done through the probability distribution:

$$P(\alpha') = p\delta(\alpha' - \alpha) + (1-p)\delta(\alpha'), \tag{1}$$

where $\delta(...)$ is the dirac delta function. Our construction works as follows; consider our starting ordered triangular lattice which has all of the bonds present. With expression (1), we are saying to take some proportion, p, of those bonds, and give them a spring constant of α. For the remaining $1-p$ bonds, give them a spring constant of 0, effectively removing or cutting them. This resulting network can be seen in the following figure:

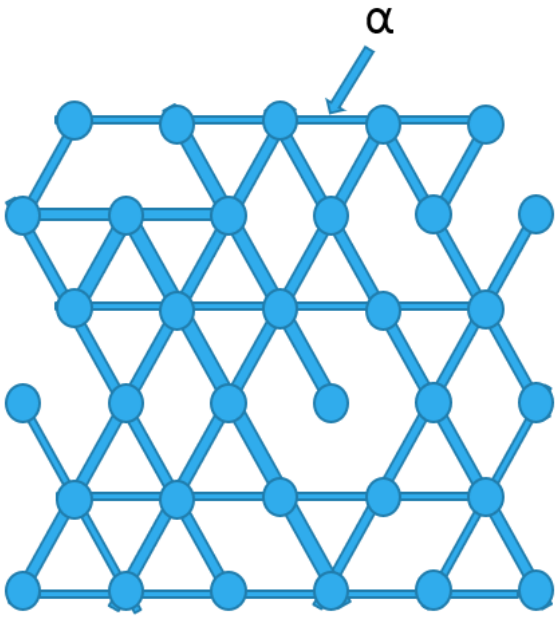

Figure 1: **Disordered Spring Network Construction**. A snapshot of a piece of the constructed network. The blue lines represent present bonds and the circles represent the crosslinker. For this construction, collections of collinear bonds are considered as one filament. Again for this version of the model the crosslinkers are placed wherever two filaments cross. With the random removal of bonds we observe how sufficient disorder is created.

We now wish to be able to make meaningful claims as to the mechanical properties of our constructed network, however attempting to do so on a disordered network can prove to be quite time consuming. Fortunately, the method we used to construct our network allows us to employ an effective

medium theory (EMT) approach to tackle this calculation. When using EMT, the disordered network of filaments which has been randomly diluted is compared to an ordered, uniform network with all the bonds present. This allows for the use of the effective ordered lattice as opposed to the original disordered structure when creating predictive models. The idea of this process is illustrated in the following figure:

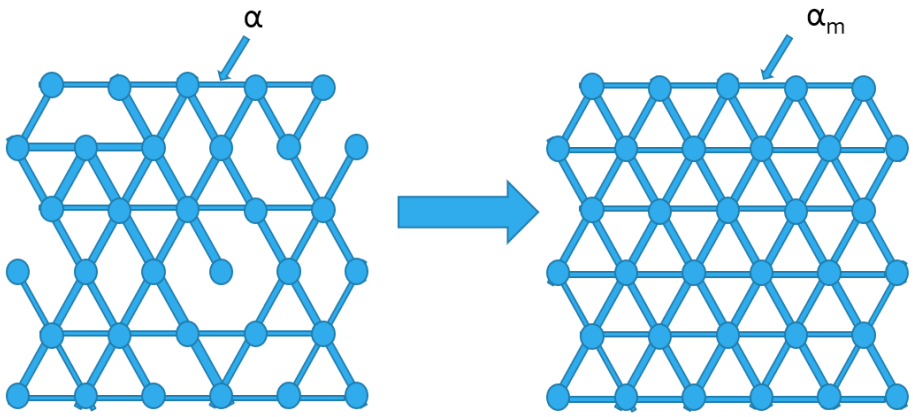

Figure 2: **Effective Medium Process**. The end goal of the process is to determine the elastic constant α_m necessary for our effective ordered lattice to exhibit the same rheological properties as the original disordered lattice.

The paper by Feng et all. details the process necessary to achieve this task, which we recreate in this paper [6]. To begin we consider our EMT ordered network. Within this network, consider two adjacent lattice points,

particularly the ones highlighted in red in Figure 3. We will refer to them as node 1 and node 2. As far as these two points are concerned, the entire network acts as one large spring between them. As such, we can represent the network using an effective spring between them. As we know each spring in the ordered network has a spring constant of α_m, we know that our effective spring constant α_{eff} between nodes 1 and 2 will be α_m/a^* [6][4][5].

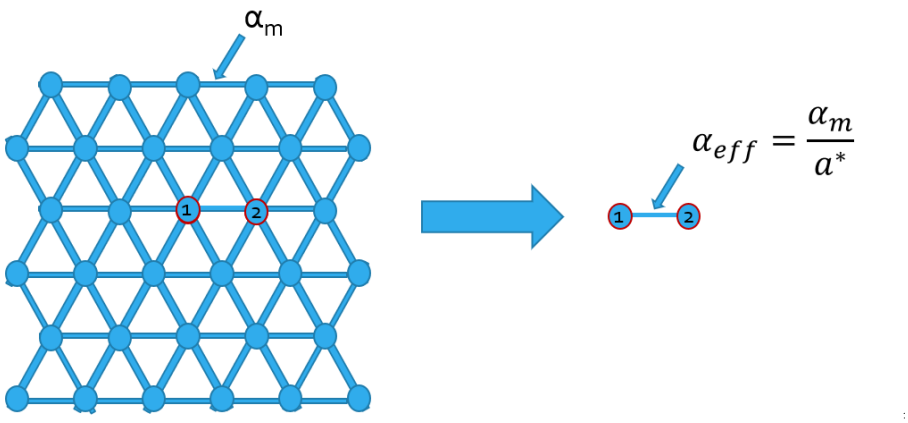

Figure 3: **Focus on One Connection**. We are focusing on just a pair of adjacent nodes. To them, the entire network acts as one large spring, represented on the right.

The parameter a^* is a geometric constant, between 0 and 1. In other words, the effective spring constant between the nodes 1 and 2 will be greater than the bare spring constant α_m because of the contribution from the net-

work, as described above in relation to α_{eff}. We will explain how we find the value of the geometric contribution a^* later, but for now we will assume we know what it is.

We would like to calculate what kind of strain fluctuations will arise in the network if we replace one bond by a spring constant of a different value. We go about finding this following the Feng et al calculation where he uses a superposition principle which says that the relative displacement between two nodes when the network is not under any stress is the same as the extra displacement between them when there is an applied uniform strain on them but no external force [6].

We apply a uniform strain to an effective network with spring constant α_m for each spring, so that all bonds are stretched by some arbitrary length $\delta\ell$. We next replace the bond between nodes 1 and 2 with a new bond with spring constant α'. If we want to bring the two nodes back to their old positions before the bond substitution, we require a virtual force $f = \delta\ell(\alpha_m - \alpha')$. To calculate the strain fluctuation, we apply this virtual force f in an unstrained network, between nodes 1 and 2 where the bond has once again been replaced by the one with spring constant α', i.e. the α_{eff} between nodes 1 and 2 is now $\alpha_m/a^* - \alpha_m + \alpha'$.

Therefore, the resulting extension or compression of the bond is given by $\delta u = \frac{f}{\alpha_m/a^* - \alpha_m + \alpha'}$, which when substituting for f yields:

$$\delta u = \frac{(\alpha_m - \alpha')\delta\ell}{\alpha_m/a^* - \alpha_m + \alpha'}. \tag{2}$$

We then ask what strain fluctuations would arise in the network, if instead of replacing just one bond, we replaced a population of bonds following the probability distribution $P(\alpha')$. The effective medium theory calculation then says that for the average response of an effective network with spring constants α_m for each spring to be the same as that of the original disordered network, these strain fluctuations should average out to 0. In other words, we can obtain an effective medium result by choosing α_m such that the average $\langle \delta u \rangle = 0$. As such, we are selecting α_m such that

$$\int \frac{\alpha_m - \alpha'}{\alpha_m/a^* - \alpha_m + \alpha'} \, P(\alpha') \, d\alpha' = 0. \tag{3}$$

.

which can be simplified to the following

$$\int \frac{P(\alpha')}{1 - a^*(1 - \alpha'/\alpha_m)} \, d\alpha' = 1. \tag{4}$$

which when solved yields

$$\frac{\alpha_m}{\alpha} = \frac{p - a^*}{1 - a^*}, \tag{5}$$

where we have replaced α' by α. This expression gives the effective medium spring constant α_m of a disordered spring network with bond occupation probability $p > a^*$ and bare spring constant α of individual springs. When $p < a^*$, the effective medium spring constant is zero.

After this derivation, expression (5) is all we will need in practice. From here we can easily compute the value of α_m in terms of the α and p from our original disordered network. The only thing left to find is the value of a^*.

From previous work [6][4][5], we are given that the value of a^* can be defined as

$$a^* = \frac{1}{3} \sum_q Tr \left[\boldsymbol{D}(q) \cdot \boldsymbol{D}^{-1}(q) \right]. \tag{6}$$

Here $\boldsymbol{D}(q)$ is the dynamical matrix for our effective network in Fourier space [6][4][5]. This dynamical matrix is a tensor which arises from the force response of our effective network. It can be thought of as the Fourier transform of a matrix of force constants. These force constants are analogues of the spring constant, but now for springs on a lattice, and can be calculated

by taking the appropriate second derivatives of the total deformation energy with respect to the displacements of the nodes in the lattice.

To explain where this dynamical matrix comes from we fist must quantify the deformation energy of our effective ordered network. Let $\hat{\boldsymbol{r}}_{ij}$ be the unit vector along bond between nodes i and j, and $\boldsymbol{u}_{ij} = \boldsymbol{u}_i - \boldsymbol{u}_j$ be the strain on the bond ij. For small deformation u, the deformation energy is the sum of the stretching energy of all the bonds present and is given by

$$E = \frac{1}{2}\alpha_m \sum_{\langle ij \rangle} \left(\boldsymbol{u}_{ij}.\hat{\boldsymbol{r}}_{ij}\right)^2 . \tag{7}$$

Using this energy expression, we can calculate the force on any given node site i as

$$F_i = \frac{\partial E}{\partial \boldsymbol{u}_i} = \sum_j \boldsymbol{D}_{ij}.\boldsymbol{u}_j, \tag{8}$$

where

$$\boldsymbol{D}_{ij} \;=\; \begin{cases} -\alpha_m \hat{\boldsymbol{r}}_{ij}\hat{\boldsymbol{r}}_{ij} & \text{if } j \neq i \\ \\ \alpha_m \sum_{j\neq i} \hat{\boldsymbol{r}}_{ij}\hat{\boldsymbol{r}}_{ij} & \text{if } j = i \end{cases} . \tag{9}$$

Notice how expression (8) bears a resemblance to Hooke's Law; we have a

force equal to something (here our dynamical matrix) times a displacement. Each element of the dynamical matrix in essence relates to a sort of spring constant pertaining to the effect of the entire network in the xx, xy, yx and yy directions respectively.

We can invert expression (8) via Fourier transformation, and when doing so our new dynamical matrix becomes

$$\boldsymbol{D}(q) \quad = \quad \alpha_m \sum_j (1 - exp(\imath q.\hat{\boldsymbol{r}}_{ij}))\hat{\boldsymbol{r}}_{ij}\hat{\boldsymbol{r}}_{ij}, \tag{10}$$

with Fourier variable q. Here $\boldsymbol{D}$(q) is the dynamical matrix in reciprocal space. Since it was derived via Fourier transformation, instead of pertaining to the entire network, now our $\boldsymbol{D}$(q) is simply taken of the the first Brilloun zone (or unit cell) of our network. For our triangular lattice, the unit cell is

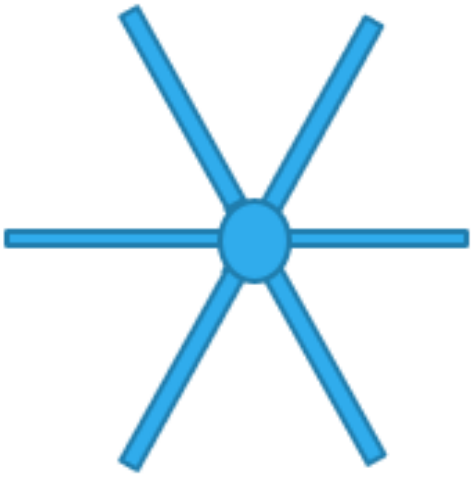

Figure 4: **Triangular Network Unit Cell**. Our unit cell for the effective medium ordered lattice. For the $\boldsymbol{D}(\mathrm{q})$, the center is node i, and the $\hat{\boldsymbol{r}}_{ij}$ represent each of the six bond directions

.

The inverse of a triangular lattice is also a triangular lattice, so our unit cell is identical in both real and reciprocal space. The unit cell is the most basic structure which can be repeated to generate the entire lattice. One can imagine how we could extend copies of our unit cell and form a full triangular lattice.

This step is also why have chosen a triangular lattice as our underlying

structure, as its unit cell has a one point basis allowing for smoother calculations. Often, a kagome lattice will be used to represent biological networks, as in these constructions only two filaments are allowed to cross at any given point, providing for far fewer bonds and a more accurate representation of the physical structures we wish to represent (as typically only two filaments will ever be crosslinked at any given point). The issue here is that the kagome lattice has a two point basis, and it is more difficult to convert to reciprocal space, making our effective medium approach much more difficult. As such we have chosen to use a triangular lattice instead, and the problem of having too many filaments crosslinked at once is accounted for in this version of the model by simply using a lover value of p in our construction. The idea here being that removing more bonds from our triangular lattice, we can reduce the likelihood of having three filaments crossing at any given point, while still maintaining the benefits of using the triangular lattice for our calculations.

We now have everything we need for our a^* from expression (6). Interestingly, as our spring case is so simple, we can actually easily see from expression (6) that a^* simply equals 2/3, even without knowing what our $\boldsymbol{D}(\mathrm{q})$ actually was. Recall that 2/3 was the value of p_{cen} for a triangular lattice of springs, so in essence $a^* = p_{cen}$. With this in mind, we can modify

our expression for our effective medium constants to be

$$\frac{\alpha_m}{\alpha} = \begin{cases} \frac{p-a^*}{1-a^*} & \text{if } p > a^* \\ 0 & \text{if } p \leq a^* \end{cases}. \tag{11}$$

This condition is how we can accurately use our effective fully ordered lattice to model our disordered construction. Recall that we said that, in our disordered version, if we have less than 2/3 of the bonds present then our network would not have enough filaments to be rigid. Now our model should be able to accurately reflect this condition, as our effective elastic constants are set to 0 if our original network is nonrigid, making our effective network nonrigid as well.

0.2.3 Semiflexible Network

A similar approach has also been shown applicable to a semiflexible network in the past, composed of filaments which require energy for both stretching and filament bending [4][5].

To create the network, we again begin with a complete triangular lattice. Wherever two filaments intersect, we place a crosslink that allows for free

rotation but prevents translation. These filaments are given a stretching spring constant, α, as well as a filament bending constant, κ, in this version. To then add sufficient disorder to the network, we again randomly remove bonds with a probability of $1 - p$. This is done through the following two probability distributions:

$$P(\alpha') = p\delta(\alpha' - \alpha) + (1 - p)\delta(\alpha') \tag{12}$$

$$P(\kappa') = p^2\delta(\kappa' - \kappa) + (1 - p_1^2)\delta(\kappa'). \tag{13}$$

These two distributions work exactly as in the spring case, however this model also contains a distribution for our new parameter κ. The main difference here that two bonds are required for any point of the lattice to experience bending, while only one bond is needed for stretching. As such, the κ expression uses p^2 in place of p. This idea is conveyed in the following figure:

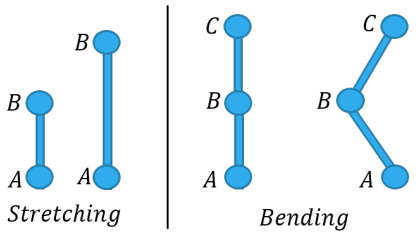

Figure 5: **Stretching and Bending**. Illustrated here is how one bond is required to represent filament stretching, where as two are required for filament bending. In our network, we consider any pair of collinear bonds to be part of a single filament. As such, on the left nodes A and B belong to 1 filament, and on the right A, B, and C all belong to the same filament. Stretching results from displacement parallel the filament. This is observed on the left, where B is being displaced away from A. Notice here that we only need to have these to nodes, and therefore 1 bond, present to illustrate this. Contrarily, bending results from displacement perpendicular to the filament direction. This is seen on the right, as B is being displaced perpendicular to the filament. As shown, we need 2 bonds present (AB and BC) to show this.

The resulting network of this construction is illustrated in Figure 6:

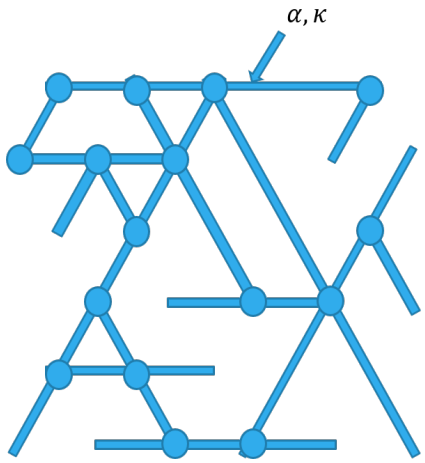

Figure 6: **Disordered Polymer Network Construction**. A snapshot of a piece of the constructed network. The blue lines represent filaments and the circles represent the crosslinker. Again for this version of the model the crosslinkers are placed wherever two filaments cross. With the random removal of bonds we observe how sufficient disorder is created.

We again wish to employ an EMT approach to this network construction to make inferences as to the mechanical properties of the network as a whole. The core idea of the process is the exact same as in the case of springs, where we wish to find an effective (ordered and complete) network which exhibits the same rheological properties as our disordered construction described above.

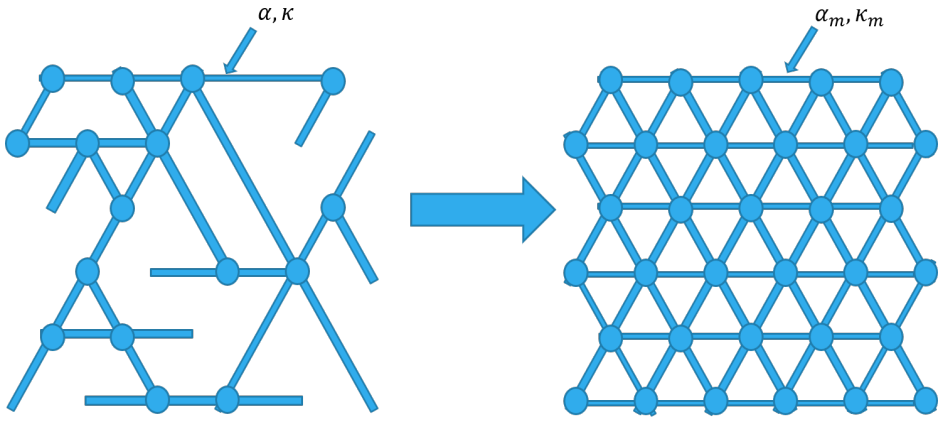

Figure 7: **Effective Medium Process**. The end goal of the process is to determine the elastic constants α_m and κ_m necessary for our effective ordered lattice to exhibit the same rheological properties as the original disordered lattice.

Much like the spring model we used, this semiflexible model is also a recreation of an existing work [4], and the paper by Das et. al. details the process necessary to derive the expressions we will use, which we will also derive in this paper. To begin, just like in the spring case, we consider our EMT ordered network. Within this network, consider three adjacent lattice points, particularly the ones highlighted in red in Figure 8. We will refer to them as nodes 1,2, and 3. We can reduce entire network to one effective filament spanning between these nodes, from the perspective of each

of the points. As we know each filament in the ordered network has a spring constant of α_m and a bending constant of κ_m, we know that our effective spring constant α_{eff} between the nodes will be α_m/a^*, and our bending constant will be κ_m/b^*. Just like before we will explicitly define a^* and b^* later, but for now we will assume we know what they are.

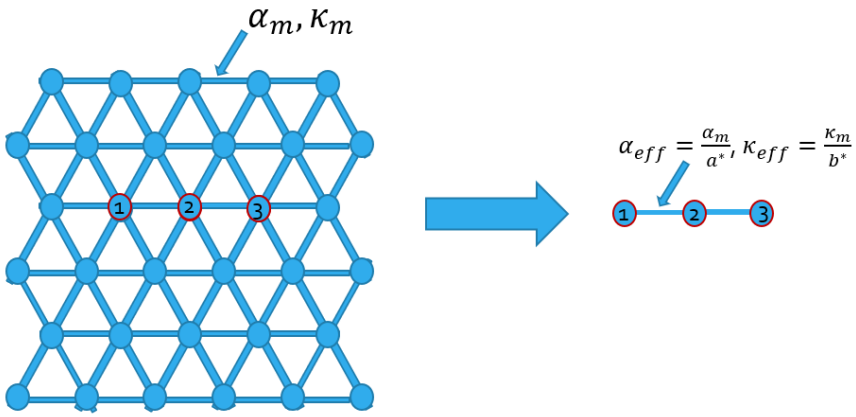

Figure 8: **Focus on One Connection**. We are focusing on just three adjacent nodes. To them, the entire network acts as one large filament, represented on the right.

We will next displace our new network of three nodes and one filament by performing two actions, both of which are are illustrated below.

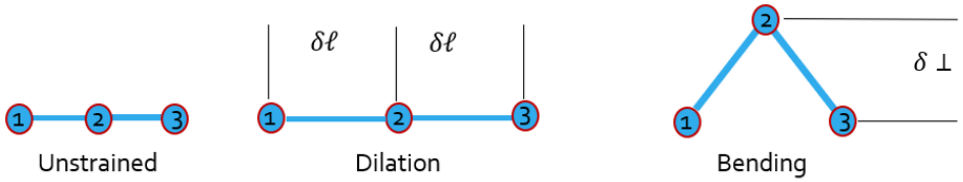

Figure 9: **Deformations**. The left shows the nodes at rest. In the center, we have dilated the network so that each bond is stretched by a given length $\delta\ell$ in a direction parallel to the filament. This is done to resemble stretching the entire filament uniformly. On the right, while maintaining the same dilation, we have bent nodes 1 and 3 downwards, displacing node 2 a distance of $\delta \perp$ perpendicular to the filament.

Now we can quantify the displacement of node 2 by breaking it down into two component directions; displacement along filament 123, and displacement perpendicular to filament 123. We can see using Hooke's Law, that the virtual force required for the displacement parallel to the filament is $2\delta\ell(\alpha_m/a^*)$, and the displacement perpendicular to the filament is achieved with a virtual force of $\delta \perp(\kappa_m/b^*)$. Assume now we replace bonds 123 in our ordered network with new bonds which has a spring constant α' and bending

constant κ', as illustrated in the figure below.

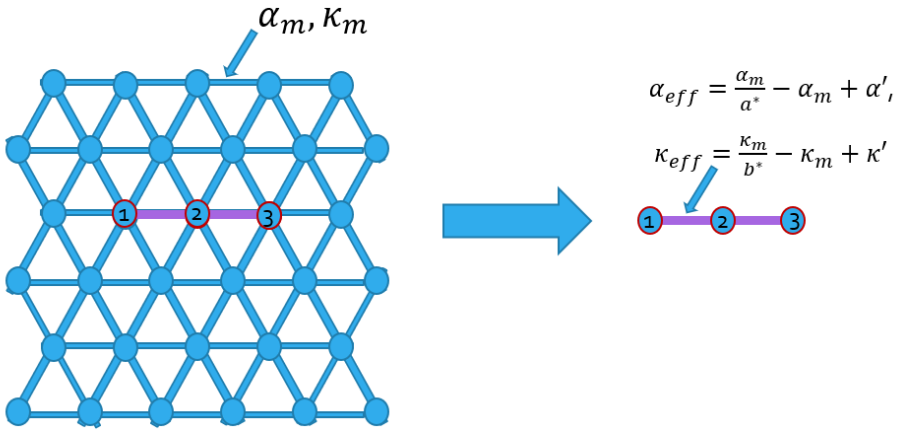

Figure 10: **Replacing the filament**. The purple bonds introduced now have a spring constant α' and bending constant κ', affecting the values of α_{eff} and κ_{eff}.

This in turn changes the value of α_{eff} and κ_{eff} to be $\alpha_m/a^* - \alpha_m + \alpha'$ and $\kappa_m/b^* - \kappa_m + \kappa'$. As such, after our substitution, to recreate the same deformation we had before, we now require a virtual force of $2\delta\ell(\alpha_m/a^* - \alpha_m + \alpha')$ for the parallel displacement and $\delta \perp(\kappa_m/b^* - \kappa_m + \kappa')$ for the perpendicular. Therefore, we can quantify the additional virtual force required now to be $f_{||} = 2\delta\ell(\alpha_m - \alpha')$ and $f_\perp = \delta \perp(\kappa_m - \kappa')$. We can then apply these force f to node 2 in an unstained version of the network, and observe a displacement of $\delta u_{||} = \frac{f_{||}}{2\alpha_m/a^* - \alpha_m + \alpha'}$, and $\delta u_\perp = \frac{f_\perp}{2\kappa_m/b^* - \kappa_m + \kappa'}$which when substituting for

f yields:

$$\delta u_{||} = \frac{(\alpha_m - \alpha')\delta\ell}{\alpha_m/a^* - \alpha_m + \alpha'} \tag{14}$$

$$\delta u_{\perp} = \frac{(\kappa_m - \kappa')\delta\ell}{\kappa_m/b^* - \kappa_m + \kappa'}. \tag{15}$$

We can now obtain our effective medium result by choosing α_m and κ_m such that the average $\langle \delta u_{||} \rangle = 0$ and $\langle \delta u_{\perp} \rangle = 0$,which can be solved independently. This ensures again that the the lattice displacement in our homogeneous effective medium material is identical to the average displacement in the spatially heterogeneous disordered material [4]. Just like in the spring case, taking this average over our probability distributions $P(\alpha')$ and $P(\kappa')$ yields our effective medium solutions, namely

$$\frac{\alpha_m}{\alpha} = \begin{cases} \frac{p-a^*}{1-a^*} & \text{if } p > a^* \\ 0 & \text{if } p \leq a^* \end{cases} \tag{16}$$

$$\frac{\kappa_m}{\kappa} = \begin{cases} \frac{p^2-b^*}{1-b^*} & \text{if } p > \sqrt{b^*}, \\ 0 & \text{if } p \leq \sqrt{b^*} \end{cases}. \tag{17}$$

Now again everything up until expressions (16) and (17) have been derivations, and these two are all we will need in practice, along with the definitions of a^* and b^*.

From previous works [4][5], we are given that a^* and b^* are determined by:

$$a^* = \frac{1}{3}\sum_q Tr\left[\boldsymbol{D}_s(q)\cdot\boldsymbol{D}^{-1}(q)\right] \tag{18}$$

$$b^* = \frac{1}{3}\sum_q Tr\left[\boldsymbol{D}_b(q)\boldsymbol{D}^{-1}(q)\right]. \tag{19}$$

Notice how these expressions look very similar to our definition of a^* used in the spring model, being again written in terms of a dynamical matrix, however for this model our dynamical matrix is derived a little differently. To illustrate this we can first describe the deformation energy of our effective medium network as follows:

Let $\hat{\boldsymbol{r}}_{ij}$ be the unit vector along bond ij, $\boldsymbol{u}_{ij} = \boldsymbol{u}_i - \boldsymbol{u}_j$ be the strain on the bond ij, and R be the lattice constant(for our calculations, we used $R = 1$. For small deformation u, the deformation energy is the sum of the stretching energy and bending energy of all the bonds present, given by:

$$E_s = \frac{1}{2}\alpha_m \sum_{\langle ij\rangle}\left(\boldsymbol{u}_{ij}.\hat{\boldsymbol{r}}_{ij}\right)^2 \tag{20}$$

$$E_b = \frac{1}{2}\kappa_m R^{-2} \sum_{\widehat{\langle hij \rangle}} \left(\boldsymbol{u}_{ih} \times \hat{\boldsymbol{r}}_{ij} - \boldsymbol{u}_{ij} \times \hat{\boldsymbol{r}}_{ih}\right)^2, \tag{21}$$

As we have two different components of our deformation energy, we will similarly have two separate components of our dynamical matrix derived from each energy expression. Specifically, from our stretching energy, E_s, we derive the stretching component of our dynamical matrix $\boldsymbol{D}_s(q)$, and likewise from the bending energy, E_b, we derive the bending component of our dynamical matrix $\boldsymbol{D}_b(q)$. Once we have derived these two components, our full $\boldsymbol{D}(q) = \boldsymbol{D}_s(q) + \boldsymbol{D}_b(q)$.

For our first component notice that our E_s is identical to the deformation energy expression from the spring model. As a result, the derivation of $\boldsymbol{D}_s(q)$ is exactly the same as our dynamical derivation from before, and we find

$$\boldsymbol{D}_s(q) \;=\; \alpha_m \sum_j (1 - exp(\imath q.\hat{\boldsymbol{r}}_{ij}))\hat{\boldsymbol{r}}_{ij}\hat{\boldsymbol{r}}_{ij}. \tag{22}$$

For our bending derivation, we will use that fact that $\hat{\boldsymbol{r}}_{ij} = -\hat{\boldsymbol{r}}_{ih}$. This comes from the idea that we have three collinear nodes, h, i, and j, with i in the middle. Therefore, the unit vector in the direction ih is in the exact opposite direction as the unit vector in the direction ij. Similarly,

we will also use $\hat{\boldsymbol{r}}_{x,ij}^2 + \hat{\boldsymbol{r}}_{y,ij}^2 = 1$, where the subscripts x and y denote the components of the vector. This equality stems from the fact that we defined $\hat{\boldsymbol{r}}_{ij}$ as a unit vector. These two equalities will be used regularly throughout the derivation, which can also be found within supplemental information for the paper written by Das et. all [4].

Our bending energy can be expanded as follows:

$$
\begin{aligned}
E_b &= (\kappa_m/2)(\boldsymbol{u}_{ij} \times \hat{\boldsymbol{r}}_{ih} - \boldsymbol{u}_{ih} \times \hat{\boldsymbol{r}}_{ij})^2 && (23)\\
&= (\kappa_m/2)[(\boldsymbol{u}_{ij} \times \hat{\boldsymbol{r}}_{ij}).(\boldsymbol{u}_{ij} \times \hat{\boldsymbol{r}}_{ij}) + (\boldsymbol{u}_{ih} \times \hat{\boldsymbol{r}}_{ih}).(\boldsymbol{u}_{ih} \times \hat{\boldsymbol{r}}_{ih}) \\
&\quad -2(\boldsymbol{u}_{ij} \times \hat{\boldsymbol{r}}_{ij}).(\boldsymbol{u}_{ih} \times \hat{\boldsymbol{r}}_{ih})] && (24)\\
&= (\kappa_m/2)[\boldsymbol{u}_{ij}^2 - (\boldsymbol{u}_{ij}.\hat{\boldsymbol{r}}_{ij})^2 + \boldsymbol{u}_{ih}^2 - (\boldsymbol{u}_{ih}.\hat{\boldsymbol{r}}_{ih})^2 - 2((\boldsymbol{u}_{ij}.\boldsymbol{u}_{ih})(\hat{\boldsymbol{r}}_{ij}.\hat{\boldsymbol{r}}_{ih}) \\
&\quad -(\boldsymbol{u}_{ij}.\hat{\boldsymbol{r}}_{ih})(\boldsymbol{u}_{ih}.\hat{\boldsymbol{r}}_{ij}))]. && (25)
\end{aligned}
$$

When further expanded, we find

$$
\begin{aligned}
E_b &= (\kappa_m/2)[(1 - \hat{\boldsymbol{r}}_{x,ij}^2)(\boldsymbol{u}_{x,ij}^2 + \boldsymbol{u}_{x,ih}^2 + 2\boldsymbol{u}_{x,ij}\boldsymbol{u}_{x,ih}) \\
&\quad +(1 - \hat{\boldsymbol{r}}_{y,ij}^2)(\boldsymbol{u}_{y,ij}^2 + \boldsymbol{u}_{y,ih}^2 + 2\boldsymbol{u}_{y,ij}\boldsymbol{u}_{y,ih}) \\
&\quad -2\hat{\boldsymbol{r}}_{x,ij}\hat{\boldsymbol{r}}_{y,ij}(\boldsymbol{u}_{x,ij}\boldsymbol{u}_{y,ij} + \boldsymbol{u}_{x,ih}\boldsymbol{u}_{y,ih} + \boldsymbol{u}_{x,ij}\boldsymbol{u}_{y,ih} + \boldsymbol{u}_{y,ij}\boldsymbol{u}_{x,ih})] && (26)
\end{aligned}
$$

From here, we can calculate our components $\boldsymbol{D}_{ii} = \frac{\partial^2 E_b}{\partial \boldsymbol{u}_{x,i} \partial \boldsymbol{u}_{y,i}}$, $\boldsymbol{D}_{ij} = \frac{\partial^2 E_b}{\partial \boldsymbol{u}_{x,i} \partial \boldsymbol{u}_{y,j}}$, $\boldsymbol{D}_{jj} = \frac{\partial^2 E_b}{\partial \boldsymbol{u}_{x,j} \partial \boldsymbol{u}_{y,j}}$, etc. This gives us

$$\boldsymbol{D}_{ii} = 4\kappa_m(\mathbf{I} - \hat{\boldsymbol{r}}_{ij}\hat{\boldsymbol{r}}_{ij}) \tag{27}$$

$$\boldsymbol{D}_{jj} = \kappa_m(\mathbf{I} - \hat{\boldsymbol{r}}_{ij}\hat{\boldsymbol{r}}_{ij}) \tag{28}$$

$$\boldsymbol{D}_{hh} = 4\kappa_m(\mathbf{I} - \hat{\boldsymbol{r}}_{ij}\hat{\boldsymbol{r}}_{ij}) \tag{29}$$

$$\boldsymbol{D}_{ij} = \boldsymbol{D}_{ji} = -2\kappa_m(\mathbf{I} - \hat{\boldsymbol{r}}_{ij}\hat{\boldsymbol{r}}_{ij}) \tag{30}$$

$$\boldsymbol{D}_{ih} = \boldsymbol{D}_{hi} = -2\kappa_m(\mathbf{I} - \hat{\boldsymbol{r}}_{ij}\hat{\boldsymbol{r}}_{ij}) \tag{31}$$

$$\boldsymbol{D}_{jh} = \boldsymbol{D}_{hj} = \kappa_m(\mathbf{I} - \hat{\boldsymbol{r}}_{ij}\hat{\boldsymbol{r}}_{ij}). \tag{32}$$

Therefore (while also dividing by two to prevent double counting),

$$\boldsymbol{D}_b(q) = 1/2 \sum \boldsymbol{D} e^{-\imath q.\hat{\boldsymbol{r}}} \tag{33}$$

$$= \kappa_m/2 \sum (4 + 1 + 1 - 2e^{-\imath q.\hat{\boldsymbol{r}}_{ij}} - 2e^{-\imath q.\hat{\boldsymbol{r}}_{ji}} - 2e^{-\imath q.\hat{\boldsymbol{r}}_{ih}} - 2e^{-\imath q.\hat{\boldsymbol{r}}_{hi}}$$

$$+ e^{-\imath q.\hat{\boldsymbol{r}}_{jh}} + e^{-\imath q.\hat{\boldsymbol{r}}_{hj}})(\mathbf{I} - \hat{\boldsymbol{r}}_{ij}\hat{\boldsymbol{r}}_{ij}) \tag{34}$$

$$= \kappa_m \sum_j [4(1 - cos(q.\hat{\boldsymbol{r}}_{ij}) - (1 - cos(2q.\hat{\boldsymbol{r}}_{ij}))](\mathbf{I} - \hat{\boldsymbol{r}}_{ij}\hat{\boldsymbol{r}}_{ij}) \tag{35}$$

Now with these expressions for the bending and stretching components of

the dynamical matrix, we have everything we need to calculate a^* and b^*, and therefore our effective medium elastic constants. Interestingly, we can also determine what we should expect our rigidity percolation threshold to be for our semiflexible model as well. Recall expressions (16) and (17). We see that to set our numerators to 0, we have $p - a^* = 0$ and $p^2 - b^* = 0$. Therefore $p^2 + p = a^* + b^*$. Notice from expressions (18) and (19), $a^* + b^* = 2/3$, which is our p_{cen} for the spring case. Therefore we have $p^2 + p = 2/3$, which when solved yields $p = 0.457$. So, when we use our semiflexible model, we should see a rigid-nonrigid transition if the p of our constructed disordered lattice is lowered below 0.457. This will be explored in the results section.

Phantom Crosslinks

After recreating two previously existing models, we have developed new construction which we will refer to as phantom crosslinks. Now the phantom construction is not completely new, as models like it have been used before in simulated networks [1][2], however it has never been applied to an effective medium construction before. This construction is identical to what we have done previously with a slight change to the crosslinker type. As mentioned in the description of our other models, our construction is based on a tri-

angular network. As such again we have the potential for up to 3 filaments to be crosslinked together by the same crosslinker. In biological networks however, this is rarely the case as we typically only observe two filaments crosslinked together. Previously, as mentioned in the spring model, to remedy this issue we simply removed enough bonds to sufficiently disorder the system and reduce the likelihood of this occurrence. This new design would provide a more holistic solution to this issue. Our phantom crosslinks will only allow for a maximum of two filaments to be linked, much like a kagome lattice construction. The third filament present will simply "pass through" the connection. This construction is illustrated in the following figure:

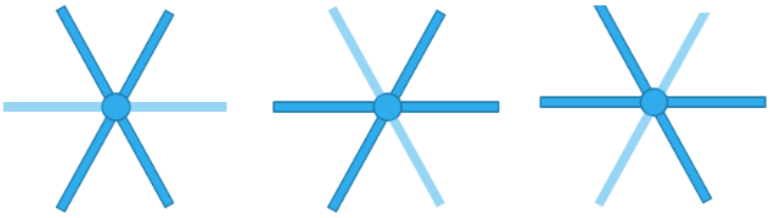

Figure 11: **Phantom Network Unit Cell**. Our construction is based off of a standard ordered triangular lattice, who's unit cell is illustrated in Figure 4. For each node, randomly two of the three filaments present are crosslinked, and the third filament simply passes through the connection. Because of this, the third filament does contribute to the deformation energy of the network as a whole, but is not visible when viewing only the unit cell (detailed later). Since the third filament is physically there, however for all intents and purposes cannot be seen by the rest of the unit cell, we refer to it as a "phantom". The three versions depicted represent the three possible unit cells which arise.

With this new construction, we find that we can maintain our desire to accurately represent biological structures which only allow for two filaments to be crosslinked at higher bond occupations than in the original spring/semiflexible models. In other words the semiflexible version of the model would be most accurate in representing single filament networks with

lower filament densities, where the phantom version can be representative of networks with much larger concentrations. Similarly, we know that in biological networks two filaments which cross are not necessarily crosslinked. In the semiflexible model, each crossing pair of filaments must be crosslinked by our construction. Our new phantom model does not have this requirement, effectively allowing us to decouple this constraint.

Now the beauty of this phantom version is since it is still fundamentally a triangular lattice only with a slightly modified crosslinker, it does not affect the construction of our disordered network, using the same probability distributions as the semiflexible model. An illustration of the phantom network construction can be seen in the following figure:

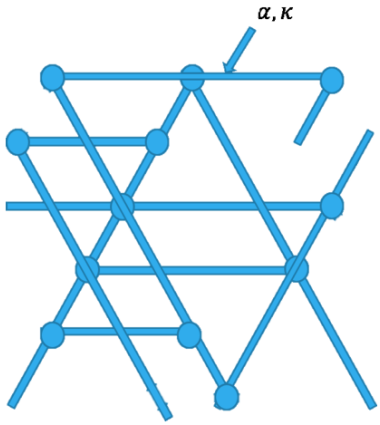

Figure 12: **Phantom Network Construction**. A snapshot of a piece of the constructed network. The blue lines represent filaments and the circles represent the crosslinkers. Notice for this model, we have the potential for filaments to simply be entangled without crosslinking, allowing for a more accurate representation of biological networks

Similarly, when employing our EMT approach to study this new construction, the derivations of our elastic constants are not affected, and we again have

$$\frac{\alpha_m}{\alpha} = \begin{cases} \frac{p-a^*}{1-a^*} & \text{if } p > a^* \\ 0 & \text{if } p \leq a^* \end{cases} \tag{36}$$

$$\frac{\kappa_m}{\kappa} = \begin{cases} \frac{p^2-b^*}{1-b^*} & \text{if } p > \sqrt{b^*}, \\ 0 & \text{if } p \leq \sqrt{b^*} \end{cases} . \tag{37}$$

Now the difference between the phantom and semiflexible models arises when computing the values of a^* and b^*. With this new version of the model, a^* and b^* are determined by:

$$a^* = \frac{1}{2} \sum_q Tr \left[\boldsymbol{D}_s(q) \cdot \boldsymbol{D}^{-1}(q) \right] \tag{38}$$

$$b^* = \frac{1}{2} \sum_q Tr \left[\boldsymbol{D}_b(q) \boldsymbol{D}^{-1}(q) \right] \tag{39}$$

Here, notice that $a^* + b^* = 1$, and our new expected rigidity percolation threshold will end up being 0.618, higher than that of the semiflexible model.

The deformation energy of this new effective medium network, namely

$$E_s = \frac{1}{2} \alpha \sum_{\langle ij \rangle} \left(\boldsymbol{u}_{ij} . \hat{\boldsymbol{r}}_{ij} \right)^2 \tag{40}$$

$$E_b = \frac{1}{2}\kappa R^{-2} \sum_{\widehat{\langle hij \rangle}} \left(\boldsymbol{u}_{ih} \times \hat{\boldsymbol{r}}_{ij} - \boldsymbol{u}_{ij} \times \hat{\boldsymbol{r}}_{ih} \right)^2 , \tag{41}$$

is still identical to the semiflexible case. As such, our resulting $\boldsymbol{D}(q) = \boldsymbol{D}_s(q) + \boldsymbol{D}_b(q)$ is identical, being determined by

$$\boldsymbol{D}_s(q) = \alpha_m \sum_j \left[1 - e^{-i\boldsymbol{q}.\hat{\boldsymbol{r}}_{ij}} \right] \hat{\boldsymbol{r}}_{ij} \hat{\boldsymbol{r}}_{ij} \tag{42}$$

$$\begin{aligned} \boldsymbol{D}_b(q) = {} & \kappa_m R^{-2} \sum_j \left[4(1 - \cos(\boldsymbol{q}.\hat{\boldsymbol{r}}_{ij})) \right. \\ & \left. -(1 - \cos(2\boldsymbol{q}.\hat{\boldsymbol{r}}_{ij})) \right] (\boldsymbol{I} - \hat{\boldsymbol{r}}_{ij} \hat{\boldsymbol{r}}_{ij}) \end{aligned} \tag{43}$$

The main difference in application lies in consideration of the unit cell. As in the semiflexible mode, these two components of the dynamical matrix are evaluated as the sum over all off the ij bonds in the unit cell, with i being the node at the center of the unit cell. In the semiflexible model, there are six such bonds, as clearly seen in Figure 4. As we now have two filaments crosslinked instead of three in each of the possible cases, the unit cell effectively cannot see the phantom filament. As a result, the summation will be done over four ij bond pairs instead of 6. As shown in Figure 11, there are three possible constructions of the unit cell, each with its own

dynamical matrix. For our purposes, we averaged over all three possibilities to determine the dynamical matrix for the overall network.

0.2.4 Composite Networks

We were further able to extend the effective medium approach to be able to represent composite disordered networks consisting of two filament types. We first construct the two disordered networks of crosslinked filaments. These two networks can be either both created with the semiflexible or phantom models, or a combination of the two. We construct two networks to represent the original disordered structures, just like in the single filament models. These filaments of each network are given a stretching spring constant, α_1 for the first and α_2 for the second, as well as a filament bending modulus κ_1 for the first and κ_2 for the second. To then add sufficient disorder to the network, we randomly remove bonds from each network with a probability of $1 - p_1$ and $1 - p_2$ respectively. This is done through the following four

probability distributions:

$$P(\alpha')_1 = p_1\delta(\alpha' - \alpha_1) + (1 - p_1)\delta(\alpha') \tag{44}$$

$$P(\kappa')_1 = p_1^2\delta(\kappa' - \kappa_1) + (1 - p_1)^2\delta(\kappa') \tag{45}$$

$$P(\alpha')_2 = p_2\delta(\alpha' - \alpha_2) + (1 - p_2)\delta(\alpha') \tag{46}$$

$$P(\kappa')_2 = p_2^2\delta(\kappa' - \kappa_2) + (1 - p_2)^2\delta(\kappa'). \tag{47}$$

Notice these are identical to what we used before, except with this construction we have created two networks instead of just one. We also chose an offset angle, θ, which is the angle the bonds of network 2 are rotated with respect to the bonds of network 1. As we wish to add some form of interaction between the networks, we then add weak connecting springs to the models. Wherever there is a bond present in the same location in each of the two networks, these bonds are then connected via a spring with spring constant α_3 connected to the midpoints to the bonds in the two networks. The idea is implemented using the probability distribution:

$$P(\alpha') = p_1p_2\delta(\alpha' - \alpha_3) + (1 - p_1p_2)\delta(\alpha') \tag{48}$$

This construction is illustrated in Figure 13.

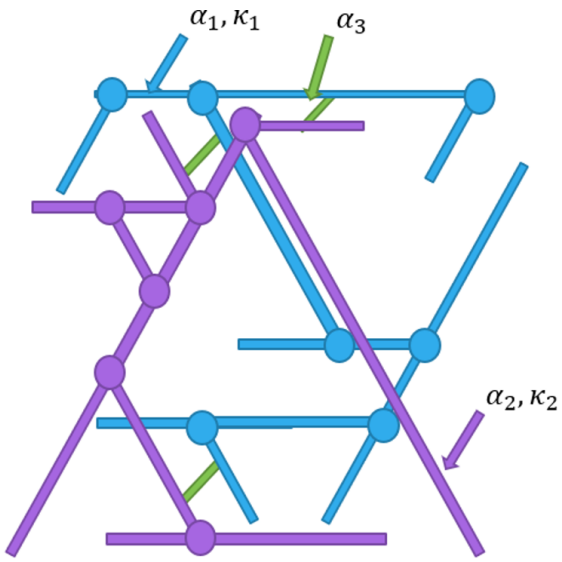

Figure 13: **Composite Polymer Network Construction Illustration**. The blue and purple filaments belong to each of the two networks while the green represent the interaction springs. With the random removal of bonds we observe how sufficient disorder is created in each network.

We can quantify the deformation energy for this composite network. Let E_1 and E_2 be the energies for each of the two networks and E_3 is the energy for the interaction springs. Let $\hat{\boldsymbol{r}}_{1,ij}$ be the unit vector along bond ij in network 1, $\hat{\boldsymbol{r}}_{2,ij}$ be the unit vector along bond ij in network 2, $\boldsymbol{u}_{1,ij} = \boldsymbol{u}_{1,i} - \boldsymbol{u}_{1,j}$ be the strain on the bond ij in network 1, $\boldsymbol{u}_{2,ij} = \boldsymbol{u}_{2,i} - \boldsymbol{u}_{2,j}$ be the strain

on the bond ij in network 2, $\hat{\boldsymbol{r}}_{3,ij} = (\hat{\boldsymbol{r}}_{1,ij} - \hat{\boldsymbol{r}}_{2,ij})/2$ be the unit vector along the connecting spring between identical bonds ij in networks 1 and 2, $\boldsymbol{u}_{3,ij} = (\boldsymbol{u}_{1,ij} - \boldsymbol{u}_{2,ij})/2$ be the strain on the connecting spring between identical bonds ij in networks 1 and 2, $R_1 = R_2 = 1$ be the lattice constants for the two networks. For small deformation u, the deformation energy is the sum of the stretching energy and bending energy of all the bonds present, given by:

$$E_1 = \frac{1}{2}\alpha_1 \sum_{\langle ij \rangle} \left(\boldsymbol{u}_{1,ij}.\hat{\boldsymbol{r}}_{1,ij}\right)^2 + \frac{1}{2}\kappa_1 R_1^{-2} \sum_{\langle \widehat{hij} \rangle} \left(\boldsymbol{u}_{1,ih} \times \hat{\boldsymbol{r}}_{1,ij} - \boldsymbol{u}_{1,ij} \times \hat{\boldsymbol{r}}_{1,ih}\right)^2 \tag{49}$$

$$E_2 = \frac{1}{2}\alpha_2 \sum_{\langle ij \rangle} \left(\boldsymbol{u}_{2,ij}.\hat{\boldsymbol{r}}_{2,ij}\right)^2 + \frac{1}{2}\kappa_2 R_2^{-2} \sum_{\langle \widehat{hij} \rangle} \left(\boldsymbol{u}_{2,ih} \times \hat{\boldsymbol{r}}_{2,ij} - \boldsymbol{u}_{2,ij} \times \hat{\boldsymbol{r}}_{2,ih}\right)^2 \tag{50}$$

$$E_3 = \frac{1}{2}\alpha_3 \sum_{\langle ij \rangle} \left(\boldsymbol{u}_{3,ij}.\hat{\boldsymbol{r}}_{3,ij}\right)^2 \tag{51}$$

$$E_{total} = E_1 + E_2 + E_3 \tag{52}$$

In the past the effective medium theory approach has been used to study networks of one filament type, however we have successfully extended the theory to cover composite networks composed of what we have described.

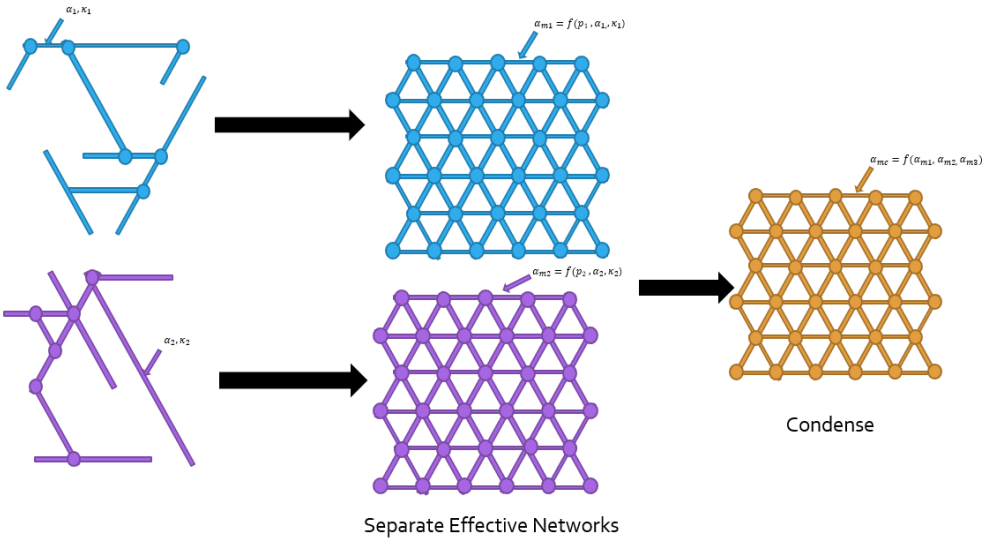

Figure 14: **Extended Effective Medium Theory**. For our new process we first find an effective medium for both networks 1 and 2. This process is completed as described in previous sections depending on which construction was chosen for the respective disordered construction for each. Once we have these two effective mediums, we can recombine the two effective mediums by adding an effective interaction spring between all of the bonds (with $\alpha_{m3} = p_1 p_2 \alpha_3$). Next we reduce this system of two combined effective networks into a mechanically equivalent ordered network of one filament type using an expression which is derived below.

As we will describe later all our our results will be measuring the shear modulus of our networks, so for our purposes, we only needed to calculate the combined stretching modulus, α_{mc} in final combined effective medium.

To determine the value of our α_{mc}, consider an identical pair of nodes ij in the effective mediums for networks 1 and 2, as illustrated in the figure below.

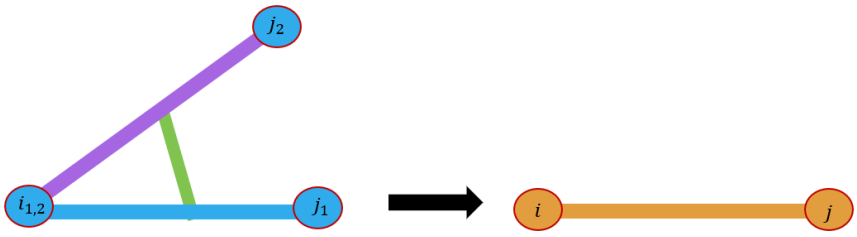

Figure 15: **Isolate 1 bond**. Here we see the versions of the same bond in networks 1 and 2. The blue filament is the bond in place in network 1 with unit vector $\hat{\boldsymbol{r}}_{1,ij}$, where the purple is the equivalent bond in network two with a unit vector $\hat{\boldsymbol{r}}_{2,ij}$. These bonds are offset by some angle θ which we chose during construction. The green filament is the connecting spring with unit vector $\hat{\boldsymbol{r}}_{3,ij}$. We wish to combine these filaments into one effective filament illustrated in orange. For simplicity, we assume the unit vector for the orange filament is the same direction as in network 1, being $\hat{\boldsymbol{r}}_{1,ij}$.

Since both of our networks are triangular lattices, we can then write our unit vectors as

$$\hat{\boldsymbol{r}}_1 = [cos(\frac{n\pi}{3}), sin(\frac{n\pi}{3})] \quad (53)$$

$$\hat{\boldsymbol{r}}_2 = [cos(\frac{n\pi}{3}+\theta), sin(\frac{n\pi}{3}+\theta)], \quad (54)$$

for some integer n. Therefore, from these two expressions, we can make the equality $\hat{\boldsymbol{r}}_2 = [cos(\theta)\hat{\boldsymbol{r}}_{1,x} - sin(\theta)\hat{\boldsymbol{r}}_{1,y}, cos(\theta)\hat{\boldsymbol{r}}_{1,y} + sin(\theta)\hat{\boldsymbol{r}}_{1,x}]$.

Now, assume we place the bonds under some uniform dilation, stretching each to a new length of $\delta\hat{\boldsymbol{r}}_1$, $\delta\hat{\boldsymbol{r}}_2$, and by extension $\delta\hat{\boldsymbol{r}}_3$. To find out what the value of our α_{mc} should be, we can equate the energy cost of doing so in both networks. In doing so we get

$$\frac{\alpha_{mc}}{2}(\delta\hat{\boldsymbol{r}}_1.\hat{\boldsymbol{r}}_1)^2 = \frac{\alpha_{m1}}{2}(\delta\hat{\boldsymbol{r}}_1.\hat{\boldsymbol{r}}_1)^2 + \frac{\alpha_{m2}}{2}(\delta\hat{\boldsymbol{r}}_2.\hat{\boldsymbol{r}}_2)^2 + \frac{\alpha_{m3}}{2}(\delta\hat{\boldsymbol{r}}_3.\hat{\boldsymbol{r}}_3)^2 \quad (55)$$

Which we can simplify to

$$\begin{aligned}\alpha_{mc}(\hat{\boldsymbol{r}}_{1,x}^2+\hat{\boldsymbol{r}}_{1,y}^2)^2 &= \alpha_{m1}(\hat{\boldsymbol{r}}_{1,x}^2+\hat{\boldsymbol{r}}_{1,y}^2)^2+\alpha_{m2}(\hat{\boldsymbol{r}}_{2,x}^2+\hat{\boldsymbol{r}}_{2,y}^2)^2 \\ &\quad +\alpha_{m3}(\hat{\boldsymbol{r}}_{3,x}^2+\hat{\boldsymbol{r}}_{3,y}^2)^2 \qquad (56)\end{aligned}$$

We know $\hat{\boldsymbol{r}}_{3,x}=(\hat{\boldsymbol{r}}_{1,x}-\hat{\boldsymbol{r}}_{2,x})/2$, $\hat{\boldsymbol{r}}_{3,y}=(\hat{\boldsymbol{r}}_{1,y}-\hat{\boldsymbol{r}}_{2,y})/2$, as well as $\hat{\boldsymbol{r}}_{2,x}=cos(\theta)\hat{\boldsymbol{r}}_{1,x}-sin(\theta)\hat{\boldsymbol{r}}_{1,y}$ and $\hat{\boldsymbol{r}}_{2,y}=cos(\theta)\hat{\boldsymbol{r}}_{1,y}+sin(\theta)\hat{\boldsymbol{r}}_{1,x}$. After making these substitutions and simplifying we find

$$\begin{aligned}\alpha_{mc}(\hat{\boldsymbol{r}}_{1,x}^2+\hat{\boldsymbol{r}}_{1,y}^2)^2 &= \alpha_{m1}(\hat{\boldsymbol{r}}_{1,x}^2+\hat{\boldsymbol{r}}_{1,y}^2)^2+\alpha_{m2}(\cos(\theta)^2+sin(\theta)^2)(\hat{\boldsymbol{r}}_{1,x}^2+\hat{\boldsymbol{r}}_{1,y}^2)^2 \\ &\quad +\alpha_{m3}(\frac{1-cos(\theta)}{2})^2(\hat{\boldsymbol{r}}_{1,x}^2+\hat{\boldsymbol{r}}_{1,y}^2)^2 \qquad (57) \\ &= \alpha_{m1}(\hat{\boldsymbol{r}}_{1,x}^2+\hat{\boldsymbol{r}}_{1,y}^2)^2+\alpha_{m2}(\hat{\boldsymbol{r}}_{1,x}^2+\hat{\boldsymbol{r}}_{1,y}^2)^2 \\ &\quad +\alpha_{m3}(\frac{1-cos(\theta)}{2})^2(\hat{\boldsymbol{r}}_{1,x}^2+\hat{\boldsymbol{r}}_{1,y}^2)^2 \qquad (58) \\ \alpha_{mc} &= \alpha_{m1}+\alpha_{m2}+\alpha_{m3}(\frac{1-cos(\theta)}{2})^2 \qquad (59)\end{aligned}$$

Which gives us an expression for α_{mc} in terms of all known quantities.

0.3 Results

0.3.1 Single Networks

We first examined the behavior of our model for each of the single network cases. As single networks have been more widely studied [6][4][5][1], we could easily be able to tell if our model was able to successfully replicate the results known from these other published models. To test out our model we chose to vary the bond occupation probability for a given network, p, and observe how the overall rigidity of the network was affected. We decided to use the shear modulus as our measurement for rigidity as this is a quantity which is measurable in lattices in a lab setting, and therefore could be useful in providing comparisons between our predictions and actual physical networks in the future. Given the use of our effective medium approach, even though our measurements are being taken using our effective ordered network, we should still observe the expected rigid-nonrigid transition as the bond occupation is decreased below the rigidity percolation threshold.

Our spring model was the first to be implemented as it provides the most simple case for comparison, the results of which can be seen in the following figure.

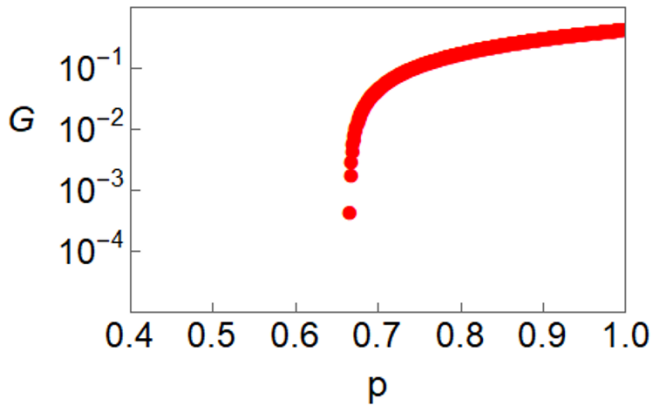

Figure 16: **Flexible Single Network** The spring model was used, placing a free-rotating crosslinker at each point where filaments cross. Here we set our theoretical $\alpha = 1$ and there is no κ in this model. This means there is no energy requirement to filament bending, so our network is completely flexible.

Observe that as we lower p, our shear modulus steadily decreases, and we see the rigid-nonrigid transition occurs at$p = 2/3$. Recall earlier that we calculated our $p_{cen} = 2/3$, so our model is behaving exactly as expected. Similarly, the paper which this model was recreated from also indicates the transition occurs at $2/3$, corroborating our results [6].

Once we verified that the model was able to correctly resemble the behavior a fully flexible network, we tested the behavior when using the semiflexible

construction. It is know that with the addition of filament bending, the network is able to maintain rigidity at a lower bond occupation than a purely flexible case. Recall that we have calculated earlier that we expect to see a transition now at $p = 0.457$, and as such should observe this behavior in our model. The results of our semiflexible test can be seen in the following figure.

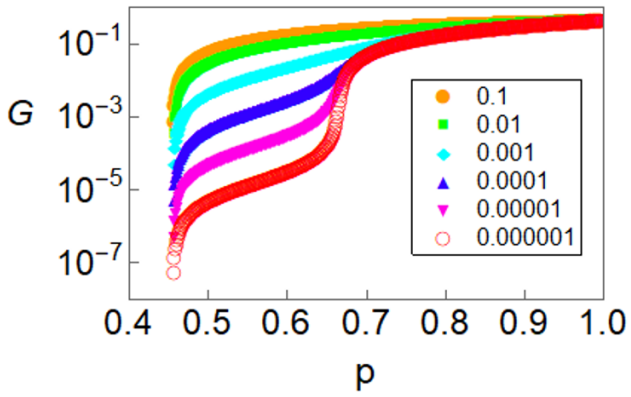

Figure 17: **Semiflexible Single Network** The basic version of the model was again used. Here we kept our theoretical $\alpha = 1$ for simplicity. We varied the value of κ for each run, represented by each of the different colors in the plot.

Observe that as we lower p, the rigid-nonrigid transition occurs at roughly $p = 0.45$, again as expected [4]. With this model, there is also notable changes

in how the model behaves as we change the value of κ. It is known that, in networks composed of semiflexible filaments, there are two distinct observable regimes; the region where the rigidity is dominated by the stretching energy costs, and the region where the bending dominates. Not by coincidence, the transition between the two regions lies at the p_{cen} for the flexible version of the network (or a network of springs of the same construction) [4][5]. We know for our case that this transition then occurs at $p = 2/3$. Notice in the above figure that for the plots where the ratio of κ/α is close to 1, we see a steady decrease in G as we reduce p. In other words there is not a noticeable transition as we change regimes. Conversely, for the plots where the ratio of κ/α is quite small, we see a noticeable inflection around the $p = 2/3$ mark. Observing this phenomenon means our model is successfully able to capture this important behavior.

Having verified that our model can accurately replicate and capture the rheological properties of the semiflexible case, we then implemented our phantom crosslink construction. Previous work has shown through simulation that networks of this construction typically exhibit a rigidity percolation threshold of around 0.618, a fact which we also calculated previously [3][1], however this is the first model which an EMT approach has never been used to model

before. For this model (and for all subsequent), we will normalize our shear modulus by the shear modulus when $p = 1$. Our results can be seen in the following figure.

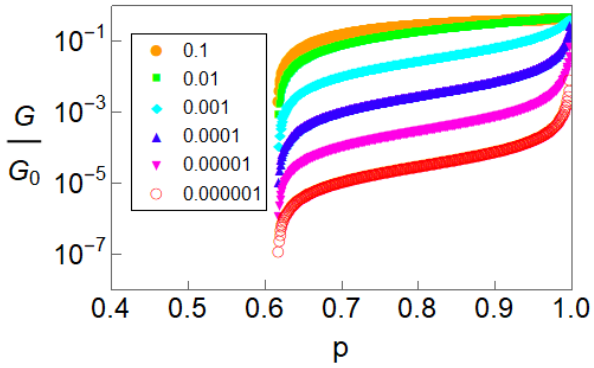

Figure 18: **Phantom Single Network** We again kept our theoretical $\alpha = 1$ for simplicity, with the different colors corresponding to values of κ.

Observe that as we vary p, the rigid-nonrigid transition occurs at roughly $p = 0.62$ Therefore we see the new phantom network model behaves as expected. Notice again that we are able to capture the regime change as well. We have stated before that the p_{cen} for the flexible case is 1 for this model, as opposed to the 2/3 of the previous case. As such, we are seeing the infection appearing near $p = 1$ now, indicating the regime change occurring at this new, correct value p. Therefore, we have successfully extended the effective medium approach to a single network consisting of phantom crosslinkers.

0.3.2 Composite Networks

After verifying the behavior of each of the single network cases individually, the next step was the implementation of our various composite network cases. The first case we chose to model was a composite network composed of two disordered latices constructed using the semiflexible model. Again we chose to use the shear modulus as our measurement for rigidity, and explored the impact of varying the bond occupation of each of the two filaments that make up the two component networks.

To test our model we chose to construct a network composed of one stiffer filament coupled with a softer filament. For each of the following tests, filament one will always be chosen to be stiffer than filament two for simplicity. We chose to fix the bond occupation of the more flexible filaments, and observe the behavior of the composite network as the bond occupation is varied for the stiffer filaments. We have selected two values for each network configuration to fix the the bond occupation of the flexible network to; marginally above the percolation threshold for the specific network (so 0.5 for the semiflexible and 0.65 for the phantom), and 0.7, an arbitrary p where most of the bonds are present. With such varied values of filament density, we should be able to clearly observe the impact the strength of the softer network has on

the composite structure by comparing the two cases. The results of the first tests can be seen in the following figure.

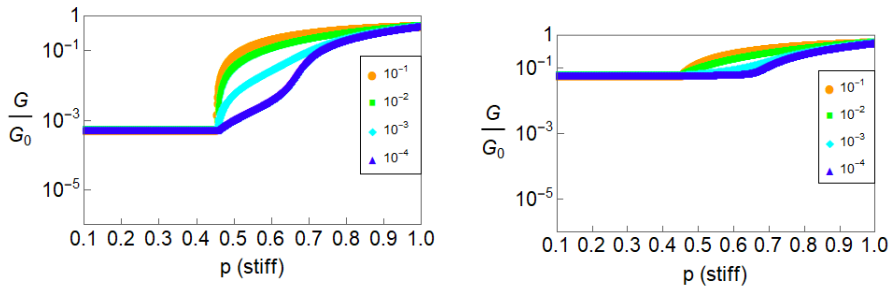

Figure 19: **Semiflexible Composite Network** For each of these tests $\alpha_1 = \alpha_2 = 1$, $\alpha_3 = 10^{-5}$, and $\kappa_2 = 10^{-4}$. The value of κ_1 is represented by each color. The value of p_2 was fixed to 0.5 on the left (0.05 above the percolation threshold for the standard crosslinker network) and 0.7 on the right.

When $p_2 = 0.5$, we see that the flexible filament network has a minimal impact on the composite whole, as the network is barely rigid with an extremely low normalized shear modulus of magnitude 10^{-3}. While there are too few stiff filaments in the system to form a rigid network, $p_1 < 0.457$, the behavior is dominated by our flexible network. If $p_1 > 0.45$, however, we observe a complete shift and the strength of the composite structure is heavily dominated by the stiffer filaments. Contrarily, when we add more of the flexible filaments to the system, the strength of the composite network

is noticeably impacted by the flexible network for much higher values of p_1. Furthermore, for weaker κ_1, we see that network 1 needs to have a high enough p_1 to enter into its stretching regime to start having a large impact on the overall rigidity. Overall, as each of the two individual networks is made stronger, the composite network as a whole is stronger, which is the result we expected to see.

The model was then used to analyze the case where both the stiff and flexible networks are constructed using the phantom crosslinkers. The results are presented in the following figure.

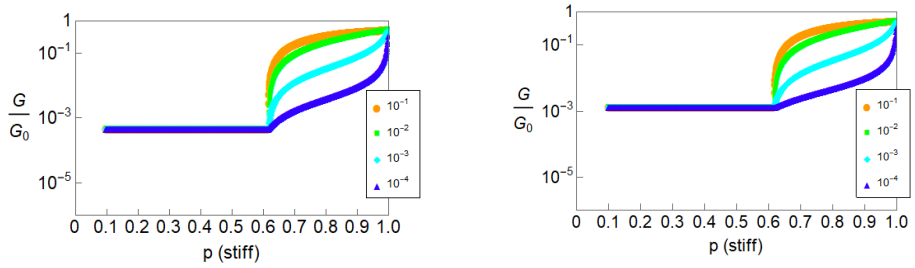

Figure 20: **Phantom Composite Network** For each of these tests $\alpha_1 = \alpha_2 = 1$, $\alpha_3 = 10^{-5}$, and $\kappa_2 = 10^{-4}$. The value of κ_1 is represented by each color. The value of p_2 was fixed to 0.65 on the left (0.05 above the percolation threshold for the phantom crosslinker network) and 0.7 on the right.

With this case we see a similar trend as was observed in the previous case,

however here the new threshold for the stiff network is 0.618. Most notable here however, the composite network is generally weaker than when using the semiflexible construction overall. A more in depth comparison between the models was later performed to further explore this comparison.

The remaining cases to which the model can be applied to are both cases where the flexible and stiffer networks each contain different crosslinker types, i.e when one network is phantom and the other is not. The results of these two cases can be seen below:

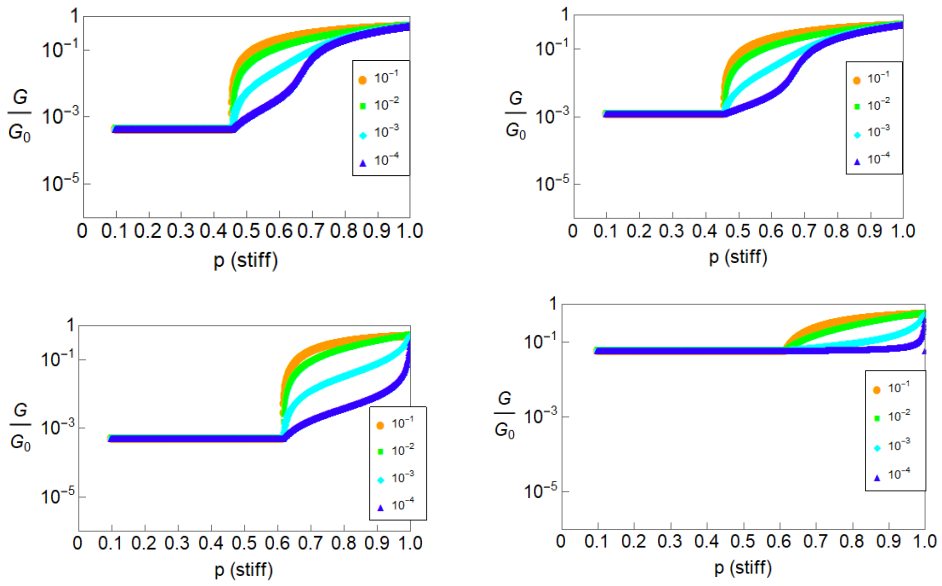

Figure 21: **Mixed Composite Network** For each of these tests $\alpha_1 = \alpha_2 = 1$, $\alpha_3 = 10^{-5}$, and $\kappa_2 = 10^{-4}$. The value of κ_1 is represented by each color. The value of p_2 was fixed to 0.65 on the top left , 0.5 on the bottom left, and 0.7 for both on the right.

As can be clearly seen in Figure 13, for low values of p_1, when the stiff network is of the phantom construction and the softer is semiflexible appears to be consistently stronger, however the same cannot easily be claimed for higher bond occupations from these tests alone.

To better compare these four network structures across all bond occupations, we have also created four phase plots. For each of these plots, we

explore how the normalized shear modulus is impacted when the bond occupation of both the stiff and more flexible networks are varied. The results can be seen in the following figure:

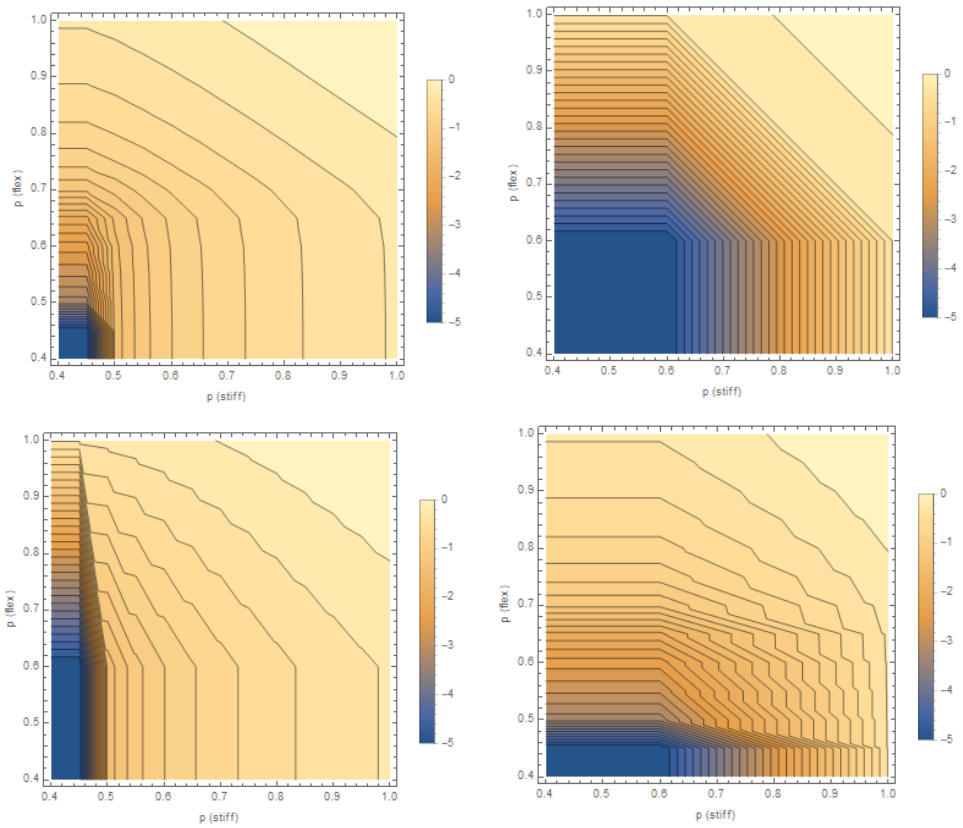

Figure 22: **Phase Plots** For each of these tests $\alpha_1 = \alpha_2 = 1$, $\alpha_3 = 10^{-5}$, $\kappa_1 = 10^{-2}$, and $\kappa_2 = 10^{-4}$. The value of the normalized shear modulus is denoted by the color bar. The top row represents the cases where both networks are created using the same model, left being both the basic model and the right being both phantom. The bottom row is the mixed cases, with the left having the stiffer network be basic, and the right having the stiffer network be phantom.

From these phase diagrams we can make a direct comparison as to the strength of all four constructions. As expected, we observe that the case where both the stiff and softer networks are made with the semiflexible model, we see the steepest increase in strength as we increase both ps, and the case where both are phantom shows the slowest increase. We can also see in both of the homogeneous construction plots, increasing the number of bonds in the stiff network has a higher impact than increasing the bonds in the softer, however this is not the case with the two mixed cases. It appears that the strength afforded by the semiflexible model is enough to override the difference in individual filament strength, for in both of the cases we see that increasing the number of bonds in the phantom network has a lesser impact on overall rigidity than for the normal semiflexible network.

0.4 Conclusion

Our initial goal was to devise a model which could be used to make predictions about various cytoskeletal-like networks, which could be solved analytically. Using previous work involving an effective medium approach, we were successfully able to adapt a model for a disordered network of one filament

type, and were able to expand it into two important new directions. Firstly, we were able to remove a fundamental restriction, which stated that whenever two filaments crossed they must be crosslinked. Through the creation of our phantom network we were able to decouple the crossing and crosslinking of filaments, providing for an entire new type of network model which was previously only possible through simulation. Secondly, we were able to expand the model to be applicable to networks of more than one filament type, thereby being applicable to our cytoskeletal structures of interest.

For our we purposes have tested our model to examine how the shear modulus is affected by the changing bond occupation probability p in our networks. This was our chosen variable as it made for easy comparison between our results and those from previous theoretical works. As for comparisons to experiments, while the bond occupation probability p is not a readily measurable quantity, as shown in [4], it can be mapped to the average filament length using $\langle L \rangle = pR(2-p)/(1-p)$ where R is the lattice constant. As such, we can then map our results of the effective elastic moduli as a function of p to a function $\langle L \rangle$ for networks of interest.

Our work provides the potential for applications in the creation of synthetic cyto-skeletal structures. Specifically, our presented model allows for

the analyzing the potential rheological properties of various network constructions given desired polymer/polymers and crosslinker types. This allows for the creation of networks with specific desired strengths, or the comparison between potential structures to see which has the more desirable outcome without the need to spend materials or extensive computational resources.

Bibliography

[1] C. P. Broedersz and F. C. MacKintosh. Molecular motors stiffen non-affine semiflexible polymer networks. *Soft Matter*, 7(7):3186, 2011.

[2] C. P. Broedersz, M. Sheinman, and F. C. MacKintosh. Filament-Length-Controlled Elasticity in 3d Fiber Networks. *Physical Review Letters*, 108(7):078102, February 2012.

[3] Chase P. Broedersz and Fred C. MacKintosh. Modeling semiflexible polymer networks. *Reviews of Modern Physics*, 86(3):995–1036, July 2014. arXiv: 1404.4332.

[4] Moumita Das, F. C. MacKintosh, and Alex J. Levine. Effective Medium Theory of Semiflexible Filamentous Networks. *Physical Review Letters*, 99(3):038101, July 2007.

[5] Moumita Das, D. A. Quint, and J. M. Schwarz. Redundancy and Cooperativity in the Mechanics of Compositely Crosslinked Filamentous Networks. *PLoS ONE*, 7(5):e35939, May 2012.

[6] Shechao Feng, M. F. Thorpe, and E. Garboczi. Effective-medium theory of percolation on central-force elastic networks. *Physical Review B*, 31(1):276, 1985.

[7] Mikkel H. Jensen, Eliza J. Morris, and David A. Weitz. Mechanics and dynamics of reconstituted cytoskeletal systems. *Biochimica et Biophysica Acta (BBA) - Molecular Cell Research*, 1853(11):3038–3042, November 2015.